

Electrochemical Imaging of Diffusion through Single Nanoscale Pores

Julie V. Macpherson,* Claire E. Jones, Anna L. Barker, and Patrick R. Unwin

Department of Chemistry, University of Warwick, Coventry CV4 7AL, U.K.

A combined scanning electrochemical-atomic force microscope (SECM-AFM) has been used to probe the diffusional transport of target electroactive solutes in isolated nanopores of a track-etched membrane. A polycarbonate membrane (100-nm-diam pore size) hydrated with an electrolyte solution, containing a redox-active probe molecule, such as IrCl_6^{3-} or $\text{Fe}(\text{phen})_3^{2+}$, functions as the model membrane system. The use of a mobile Pt-coated AFM probe enables individual solution-filled pores to be topographically identified. Analysis of the corresponding current images for the diffusion-limited oxidation of the redox mediator indicates that solution is largely confined to pores in the membrane. Moreover, the tip collector current response provides information on diffusion of the mediator through the pore. Force–distance tip approach and retract measurements allow the radius of contact between the electrochemical-AFM tip and solution confined within a pore at the point of pull-off to be estimated.

The transport of chemical species through pores and channels is important in many areas,^{1–3} ranging from ion transport through membrane channels to catalytic reactions in zeolites and other nanoporous solids. As the size of a pore shrinks to the nanoscopic scale, factors such as the surface chemistry of the pore wall and the size of the molecule become increasingly important.^{4,5} To date, various methods have been employed to characterize transport processes across nanoporous membranes, including gas permeation experiments,^{4,6} coulter particle counting,⁷ and patch clamping.⁸

To obtain a quantitative description of transport in nanoporous systems, measurements should ideally be made under well-defined

conditions. Recent model candidates have included monodisperse porous membranes that contain arrays of nanopores,^{9–14} such as track-etched polycarbonate membranes,⁹ porous alumina membranes,¹⁴ carbon nanotube arrays,¹³ and membranes formed from templating media, for example, latex spheres^{10,11} and block copolymers.¹² Hitherto, transport measurements on these membranes have tended to be time- or pore-density-averaged, given that many pores are usually sampled simultaneously. To address a single pore, Crooks and Sun have reduced the templating methodology to a single, nonrepeatable structure using either a glass fiber¹⁵ or a multiwalled carbon nanotube¹⁶ to form the pore. Other work has seen the ion-track-etching process decreased to a level of only 1 pore/membrane.¹⁷

In this paper, we describe a novel procedure for the investigation of diffusion processes through single pores at the nanoscopic level. The methodology derives from earlier work in our group in which a Pt-coated atomic force microscope (AFM) probe was shown to be capable of functioning as both an electrode and a force sensor.^{18,19} The nanoporous system consists of an array of 100-nm (nominal)-diam track-etched pores in a commercially available polycarbonate membrane. The pores are wetted and filled from below by an electrolyte solution containing a redox mediator. By using the probe as a moveable topographical and electrochemical sensor, we are able to address individual solution-filled pores. With a second electrode placed in solution beneath the membrane, electrical contact is made when the tip comes into contact with solution, resulting in a closed electrochemical cell. With this arrangement, we are thus able to probe the diffusional response of a mediator species in a single nanoscale pore. Given the dimensions of the pores employed (10- μm long, 100-nm diam) the geometry of the tip in contact with solution confined in the

* j.macpherson@warwick.ac.uk.

- (1) (a) Matsuda, H.; Saigusa, A.; Irisawa, H. *Nature* **1987**, *325*, 156. (b) Goulding, E. H.; Tibbs, G. R.; Liu, D.; Siegelbaum, S. A. *Nature* **1993**, *364*, 61.
- (2) Reyes, S. C.; Sinfelt, J. H.; DeMartin, G. J. *J. Phys. Chem. B* **2000**, *104*, 5750.
- (3) Davis, M. E. *Micro. Meso. Mater.* **1998**, *21*, 173.
- (4) Hulteen, J. C.; Jirage, K. B.; Martin, C. R. *J. Am. Chem. Soc.* **1998**, *120*, 6603.
- (5) Jirage, K. B.; Hulteen, J. C.; Martin, C. R. *Anal. Chem.* **1999**, *71*, 4913.
- (6) Petzny, W. J.; Quinn, J. A. *Science* **1969**, *166*, 751.
- (7) Lines, R. W. In *Particle Size Analysis*; Stanley Wood, N. G., Lines, R. W., Eds.; Royal Society of Chemistry: Cambridge, 1992.
- (8) Ogden, D., Ed. *Microelectrode Techniques*; The Company of Biologists Limited: Cambridge, 1987.

- (9) Martin, C. R. *Science* **1994**, *266*, 1961.
- (10) Holland, B. T.; Blandford, C. F.; Stein, A. *Science* **1998**, *281*, 538.
- (11) Antonietti, M.; Berton, B.; Goltner, C.; Hentze, H. P. *Adv. Mater.* **1998**, *10*, 154.
- (12) Templin, M.; Franck, A.; DuChesne, A.; Leist, H.; Zhang, Y. M.; Ulrich, R.; Schädler, V.; Wiesner, U. *Science* **1997**, *278*, 1795.
- (13) Miller, S. A.; Young, V. Y.; Martin, C. R. *J. Am. Chem. Soc.* **2001**, *123*, 12335.
- (14) Dalvie, S. K.; Baltus, R. E. *J. Membr. Sci.* **1992**, *71*, 247.
- (15) Sun, L.; Crooks, R. M. *Langmuir* **1999**, *15*, 738.
- (16) Sun, L.; Crooks, R. M. *J. Am. Chem. Soc.* **2000**, *122*, 12340.
- (17) Reber, N.; Küchel, A.; Spöhr, R.; Wolf, A.; Yoshida, M. *J. Membr. Sci.* **2001**, *193*, 49.
- (18) Macpherson, J. V.; Hillier, A. C.; Unwin, P. R.; Bard, A. J. *J. Am. Chem. Soc.* **1996**, *118*, 6445.
- (19) Jones, C. E.; Macpherson, J. V.; Barber, Z. H.; Somekh, R. E.; Unwin, P. R. *Electrochem. Comm.* **1999**, *1*, 55.

mouth of the pore is unimportant. The electrode serves only to induce and measure diffusion of electroactive species through the pore.

The studies in this paper build primarily on two aspects of prior work in scanning electrochemical microscopy (SECM). First, SECM has been employed to investigate diffusive,²⁰ convective,²¹ and migrational²² transport across porous materials, primarily at the micrometer (and larger) level. There has been one report of SECM iontophoretic studies using smaller-sized pores (~100 nm); however, given that radial diffusion prevails on the exit side of the membrane, the resolution was much lower.^{22c} This was further compounded by the comparatively large tip electrodes employed for imaging. Second, SECM in-air imaging in humid environments has been employed for high-resolution topographical measurements.²³ By using combined SECM-AFM, we show in this paper that structure–activity problems can readily be investigated at high spatial resolution. Simultaneous measurements of the adhesion force between the Pt-coated AFM tip and the solution enable the contact area between the tip and solution confined within a pore to be estimated.

EXPERIMENTAL SECTION

Materials. All solutions were prepared from Milli-Q reagent water (Millipore Corp). Solutions contained either potassium hexachloride iridate(III) (IrCl_6^{3-} , Sigma Aldrich) at a concentration of 10 mM in 0.5 M potassium nitrate (Fisons, AR) or tris 1,10-phenanthroline iron(II) sulfate ($\text{Fe}(\text{phen})_3^{2+}$, BDH) at a concentration of 10 mM in 0.5 M potassium chloride (Fisons, AR grade).

Circular samples of polycarbonate track-etched ultrafiltration membrane (Millipore) of diameter 13 mm, thickness 10 μm , and nominal pore size 100 nm were used. Hydration of the membrane was achieved by securing the porous substrate (shiny side orientated upward) over the top face of a home-built polyetheretherketone (PEEK) reservoir cell filled to the brim with the electrolyte solution. This arrangement is depicted schematically in Figure 1. A chloridised silver wire (Goodfellow) functioned as a Ag/AgCl reference electrode. This was secured in place in the solution reservoir with epoxy resin ("Araldite", Evode Ltd., Stafford, U.K.).

Instrumentation. A Nanoscope E AFM and fluid cell (Digital Instruments, Santa Barbara) was employed. The AFM was equipped with a sample scanner that facilitated a maximum scan range of $120 \times 120 \mu\text{m}$. The instrument was placed on a Newport Corp (Newbury, CT) SHP series subhertz platform which, in turn, was placed on a custom-built granite bench incorporating vibration isolators. The AFM was shielded using a home-built Faraday cage. The AFM probes (Digital Instruments; DI) consisted mainly of Si_3N_4 cantilevers with integrated pyramidal tips, although Si tips were occasionally used. The underside of the probes was sputter-

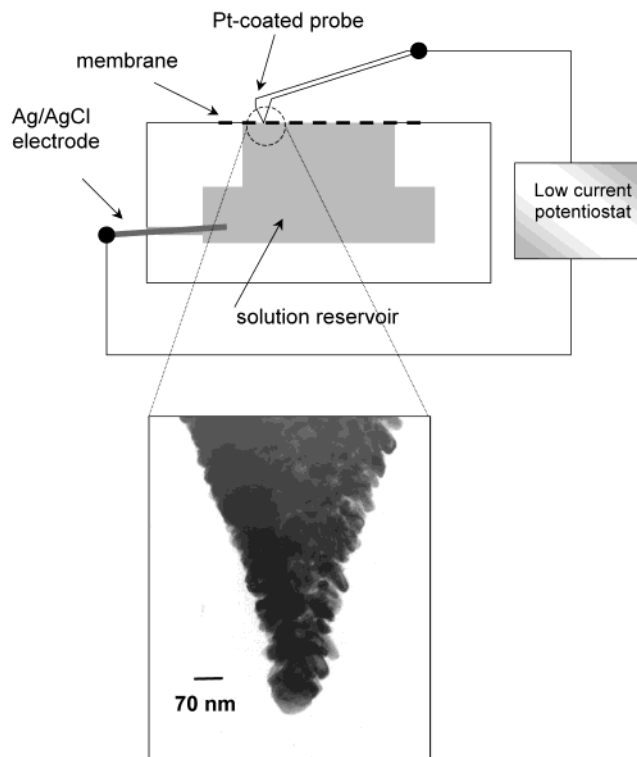


Figure 1. Schematic representation of the experimental setup for SECM-AFM imaging of wetted nanopores. The inset shows a TEM image of a typical Pt-coated Si tip.

coated, initially with Cr (3 nm) and then with Pt (50 nm), to provide conducting AFM tips capable of functioning as electrodes, as well as force sensors. This procedure was carefully optimized to produce metal-coated probes that were (i) durable; (ii) long-lasting, and (iii) coated evenly with Pt to the very end of the tip.

The inset to Figure 1 shows a typical transmission electron micrograph (TEM) of a Pt-coated Si tip. The grain structure of the Pt film is clearly visible over a significant area of the tip. There appears to be one grain covering the apex of the tip. A similar grain structure was observed by TEM for Pt-coated Si_3N_4 probes, although it was only possible to resolve the very apex of the tip because of the larger cone angle.

SECM-AFM Amperometric Measurements. Amperometric measurements employed a two-electrode setup with the Pt-coated AFM tip functioning as the working electrode, as described above. Electrical contact to the probe was made via the metal spring clasp of a commercial fluid cell holder (DI) that rested on the main body of the probe. The fluid cell was used without an O-ring to avoid any pressure-induced transport of solution through pores due to the action of clamping the O-ring onto the sample. The current was measured, and the potential was controlled using a model EI-400 bipotentiostat (Cypress Systems, Kansas) equipped with a high-gain preamplifier connected to a purpose-built triangular wave/pulse generator (Colburn Instruments, Coventry). The current was recorded directly to an auxiliary output using a signal access module (DI), allowing the simultaneous acquisition of electrochemical and topographical data by the AFM instrumentation. Cyclic voltammograms (CVs) were recorded directly on a PC equipped with a data acquisition card (Lab-PC-1200, National Instruments Corp. Ltd., UK) using software written in-house.

(20) Nugues, S.; Denuault, G. *J. Electroanal. Chem.* **1996**, *408*, 125.

(21) (a) Macpherson, J. V.; Beeston, M. A.; Unwin, P. R.; Hughes, N. P.; Littlewood, D. *Langmuir* **1995**, *11*, 3959. (b) Macpherson, J. V.; Beeston, M. A.; Unwin, P. R.; Hughes, N. P.; Littlewood, D. *J. Chem. Soc., Faraday Trans.* **1995**, *91*, 1407.

(22) For example, see: (a) Bath, B. D.; Lee, R. D.; White, H. S. *Anal. Chem.* **1998**, *70*, 1047. (b) Lee, R. D.; White, H. S.; Scott, E. R. *J. Pharm. Sci.* **1995**, *85*, 1186. (c) Scott, E. R.; White, H. S.; Phipps, J. B. *Anal. Chem.* **1993**, *65*, 1537.

(23) (a) Fan, F. R.-F.; Bard, A. J. *Science* **1995**, *270*, 1849. (b) Forouzan, F.; Bard, A. J.; *J. Phys. Chem. B* **1997**, *101*, 10876. (c) Fan, F. R.-F.; Bard, A. J. *Proc. Natl. Acad. Sci.* **1999**, *96*, 14222.

Tip Approach Measurements. Approach curve measurements were typically made at a scan rate of 0.1 Hz over a distance of $\sim 1 \mu\text{m}$ with the tip aligned directly over a pore. For these measurements, the tip was held in position by reducing the scan size to $0 \times 0 \text{ nm}$ and disabling the slow-scan axis. As the substrate was translated toward and away from the Pt-coated AFM tip, the current and tip deflection data were usually acquired simultaneously, with the tip biased at a potential sufficient to electrolyze the solution mediator confined within the hydrated pores at a diffusion-limited rate.

Tip Shape Characterization and Cantilever Calibration.

The radius of curvature, R_t , of Pt-coated AFM tips was determined using a custom-built tip imaging grid.²⁴ Typically, R_t values in the range $55 \pm 10 \text{ nm}$ were determined, although in some instances, R_t values as large as 110 nm were obtained. For the experiments described herein, the sharper tips were preferred. Variations in R_t arising from both a nonuniformity in the metal deposition process and in the microfabrication procedure²⁵ are common in both uncoated and coated Si_3N_4 tips. The spring constant, k , of the metal-coated cantilevers was measured using a resonance detection method²⁶ in which small spheres of borosilicate glass ($\sim 14.5\text{-}\mu\text{m}$ diam, $\sim 4 \text{ ng}$; Duke Scientific, CA) were placed on the end of the lever on the same side as the integrated tip using a sharpened length of tungsten wire. The resonance frequency of the cantilever was determined by monitoring the signal from the photodiode detector with a spectrum analyzer (Stanford Research Systems, model SR760, CA).

Contact Angle Measurements. Contact angles were measured using a horizontally mounted stereo zoom microscope (model 700-Z, Motic) with a CCD color video camera (model TK-C601, JVC) coupled to a monitor and video recorder. For these measurements, a small drop ($\sim 10 \mu\text{L}$) of electrolyte solution (0.5 M KNO_3) was placed onto the surface of interest, followed immediately by a second drop to the initial volume of solution while continuously recording the procedure on video. Subsequent analysis of the image recorded immediately after the second drop of solution had been added enabled a value for the contact angle, θ , on the surface of interest to be obtained.

RESULTS AND DISCUSSION

Simultaneous Topography and Electrochemical Imaging.

Figure 2, parts a and b, respectively, show the height and current images of a track-etched polycarbonate membrane hydrated with an electrolyte solution containing 10 mM IrCl_6^{3-} and 0.5 M KNO_3 that were recorded simultaneously with a Pt-coated AFM tip in contact mode. The tip was scanned from left to right (fast-scan axis) and from top to bottom (slow-scan axis). The scan size was $2.5 \times 2.5 \mu\text{m}$ (composed of 256 lines), imaged at a scan rate of 1 Hz. During imaging, the tip was held at a potential of +1.0 V versus Ag/AgCl, sufficient to effect the one-electron oxidation of IrCl_6^{3-} at a diffusion-controlled rate.

Topographically, the probe is able to clearly identify the position of the nanopores in the membrane. The pores appear as

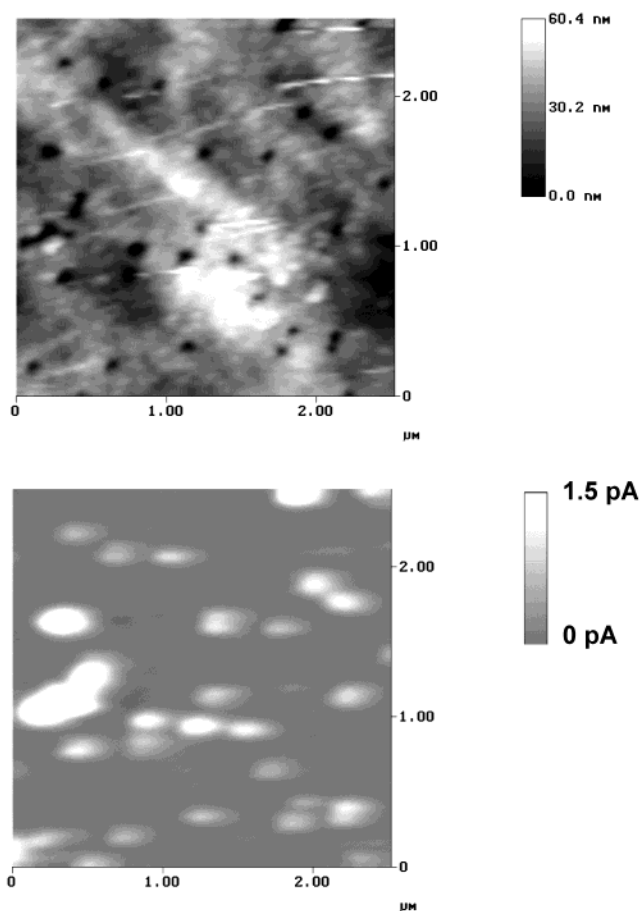


Figure 2. Height (a) and current (b) images of a wetted track-etched polycarbonate membrane acquired simultaneously with the SECM-AFM tip. The scan size was $2.5 \times 2.5 \mu\text{m}$, and data were acquired at a scan rate of $2.5 \mu\text{m s}^{-1}$ with the tip biased at +1.0 V versus Ag/AgCl. The wetting solution contained 10 mM IrCl_6^{3-} in 0.5 M KNO_3 .

dark circular pits in the height image (Figure 2a). At these locations, the electrochemical image displays bright spots, which correspond to a current, typically $< 1 \text{ pA}$, in zones where only a single pore resides. The measured currents result from the diffusion-controlled oxidation of IrCl_6^{3-} present within the nanoscopic array of solution-filled pores. The amperometric data associated with each pore has a slightly smeared appearance that is attributed to the slight displacement and dragging of fluid as the tip moves across the opening of a pore, but in general, solution is largely confined to the pores.

Diffusion can be considered the dominant mode for the mass transport of species through the pore to the electrochemical-AFM tip. With the high supporting electrolyte concentrations employed, the electrical double layers formed at the pore walls will be negligible when compared to the dimension of the pore.^{27,28} The problem thus condenses to hemispherical diffusion of mediator to the base of the pore coupled to linear diffusion through the pore. Under these conditions, the situation closely resembles that of diffusion to a recessed microdisk electrode, as shown schemati-

(24) Bykov, V.; Gologanov, A.; Shevyakov, V. *Appl. Phys. A* **1998**, *66*, 499.

(25) (a) Noy, A. N.; Frisbie, C. D.; Rozsnyai, L. F.; Wrighton, M. S.; Lieber, C. M. *J. Am. Chem. Soc.* **1995**, *117*, 7943. (b) Noy, A.; Vezennov, D. V.; Lieber, C. M. *Annu. Rev. Mater. Sci.* **1997**, *27*, 381.

(26) Cleveland, J. P.; Manne, S.; Bocek, D.; Hansma, P. K. *Rev. Sci. Instrum.* **1993**, *64*, 403.

(27) Feldberg, S.; Bard, A. J. *Anal. Chem.* **1997**, *69*, 4627.

(28) Bard, A. J.; Faulkner, L. R. *Electrochemical Methods: Fundamentals and Applications*, John Wiley: New York, 1980; p 504.

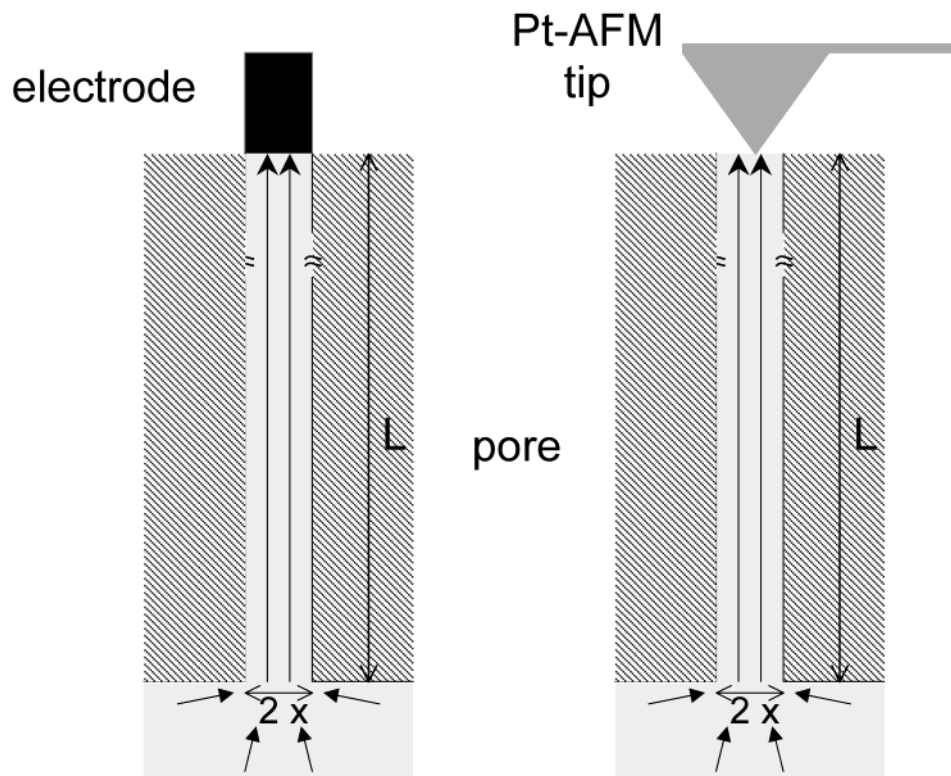


Figure 3. Schematic representation (cross section) of diffusion to an electrode located at the mouth of a pore in an arrangement analogous to a recessed microdisk electrode. The corresponding situation for diffusion to a Pt-coated AFM probe is also shown. Given the large ratio of pore length to diameter, the electrode geometry has a negligible effect on the electrode response. Contact angle measurements of the electrolyte on the surface of the polycarbonate membrane indicate that the electrolyte meniscus in the pore should be close to horizontal (82° with respect to the pore wall).

cally in Figure 3, for which eq 1 describes the limiting current.²⁹

$$i_{\text{lim}} = \frac{4\pi n F c^* D x^2}{4L + \pi x} \quad (1)$$

where L is the length of the pore ($10 \mu\text{m}$ herein), n is the number of electrons transferred per redox event, F is Faraday's constant, and D is the diffusion coefficient of the electroactive mediator ($7.5 \times 10^{-6} \text{ cm}^2 \text{ s}^{-1}$ for IrCl_6^{3-} ³⁰), which has a bulk concentration c^* . Here, x is the radius of the pore opening ($\sim 50 \text{ nm}$). Equation 1 predicts a value for $i_{\text{lim}} \approx 0.6 \text{ pA}$, which is the maximum current that the pore can sustain during diffusion-controlled electrolysis of the mediator species. It is important to note that given the dimensions of the pore, particularly the large length-to-radius ratio, the geometry of the tip in contact with solution is unimportant. Diffusion of electroactive species through the pore, for subsequent collection at the tip electrode, is the limiting process. This analysis assumes that evaporation from the pores does not lead to a change in the bulk concentration detected. This is reasonable, given that the experiments were carried out in a closed environment. Moreover, once the tip is carrying out electrolysis over a pore, the short diffusional time in this nanoscale system, compared to the measurement time, ensures that the tip sees the bulk concentration under steady-state conditions. The inherently high

diffusion times are considered below in relation to the time-dependent current response.

Under the scanning conditions employed (tip scan speed, $v = 2.5 \mu\text{m s}^{-1}$), the residence time of the tip in the vicinity of a single pore, $t_{\text{res}} = v/2x$, is $\sim 40 \text{ ms}$. Analytical expressions, eqs 2 (short time) and 3 (long time), describe the current–time behavior of a recessed microdisk electrode²⁹ following a step in the potential from a value at which no current flows to one at which the mediator species is electrolyzed at a diffusion-controlled rate.

$$i = n F c^* x^2 (\pi D / t)^{1/2} [1 + 2 \exp\{-L^2/Dt\} + 2 \exp\{-4L^2/Dt\} + \dots] \quad (2)$$

$$i = (\pi n F c^* D x^2 / L) [1 + 2 \exp\{-\pi^2 D t / L^2\} + 2 \exp\{-4\pi^2 D t / L^2\} + \dots] \quad (3)$$

These results suggest that the system will have almost attained steady-state on this time scale. Specifically, after 40 ms , the current will be within 10% of the steady-state value. These expressions are valid for $L/x > 2$,³¹ which is appropriate for this system with $L/x \approx 100$. The form of the current–time curve for the parameters herein is shown in Figure 4.

Figure 5a,b displays cross-sectional analyses of the steady-state current as the tip scans over a series of single pores. Where the pores are completely isolated from each other, the limiting steady-

(29) Bond, A. M.; Luscombe, D.; Oldham, K. B.; Zoski, C. G. *J. Electroanal. Chem.* **1988**, *1*, 249.

(30) Macpherson, J. V.; Jones, C. E.; Unwin, P. R. *J. Phys. Chem. B* **1998**, *102*, 9891.

(31) Bartlett, P. N.; Taylor, S. L. *J. Electroanal. Chem.* **1998**, *453*, 49.

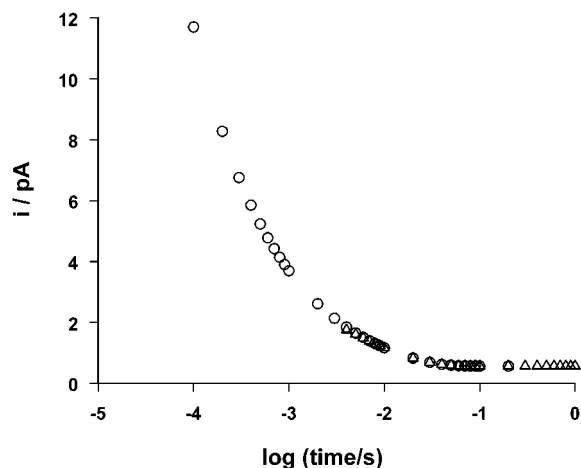


Figure 4. Theoretical current–time response at a recessed micro-disk electrode, following a step in the potential from a value where no current flows to one where electrolysis of the electroactive species occurs at a diffusion-controlled rate. The data have been derived from the short (O) and long (Δ) time limits, eqs 2 and 3 respectively [29], for the following parameters: $D = 7.5 \times 10^{-6} \text{ cm}^2 \text{ s}^{-1}$, $c^* = 10 \text{ mM}$, $L = 10 \text{ }\mu\text{m}$, and $x = 50 \text{ nm}$.

state current varies in the range 0.6–1.8 pA. This is in good agreement with the theoretically predicted current for diffusion through a single pore. Because the tip geometry is unimportant in governing the response for this membrane, variations in the magnitude of the limiting current at single pores are likely to arise from structural imperfections known to be common in track-etched membranes.³² These include a nonuniform pore length due to the tilt angle of the track etch and “cigar-shaped” pores.³² Previously reported scanning electron microscopy (SEM) images of metal electrodeposited within pores of track-etched membranes demonstrate that in many cases, the middle section of the pore is larger in diameter than the two outer ends. In some cases, the average diameter for the pore can be as much as twice the pore opening.³² Under these conditions, i_{lim} will approach a value of 2.3 pA, based on eq 1.

When pores in the membrane merge, the current response is clearly higher, as shown in Figure 5c, because of an increase in the effective pore radius. Figure 6 shows a typical cyclic voltammogram for the oxidation of 10 mM $\text{Fe}(\text{phen})_3^{2+}$ in 0.5 M KCl, confined to three overlapping pores, at a Pt-coated AFM tip. The tip potential was scanned at a sweep rate of 10 mV s^{-1} . The limiting current in this case is seen to be of the order of 5 pA.

Over 100 separate experiments were performed on solution-filled nanoporous membranes, with several different electroactive mediators (we only report data for IrCl_6^{3-} and $\text{Fe}(\text{phen})_3^{2+}$ herein). For all the mediators investigated, similar results were obtained. We have found that the contact force applied by the tip on the membrane surface is an extremely important experimental parameter. If the tip engaged with too much force or if the force applied during imaging was excessive, solution was forced from the pores and onto the surrounding membrane. Under these conditions, a nonzero baseline current was observed, and the

currents measured at single pores were many times higher than expected on the basis of eq 2.¹⁹ This is because the tip current is likely to be partially limited by mass transport within a thin layer of electrolyte above the membrane and through several pores located in the vicinity of the tip. Currents of the order of those observed in Figure 2b were seen only with the tip imaging under a minimal contact force. This also helped to preserve the structural integrity of the metal-coated tip. For example, the same tip could be used many times in different experiments before a deterioration in the current response was observed.

Approach and Retract Force Curves. Figure 7a,b shows typical cantilever deflection and limiting current data recorded simultaneously as the tip (biased at +1.0 V to effect diffusion-controlled oxidation of the mediator) was brought into contact (solid line) and retracted (dashed line) from a single pore filled with solution containing 10 mM IrCl_6^{3-} and 0.5 M KNO_3 . The electrochemical response of the approach curve effectively represents a potential step chronoamperometric experiment, with the electrochemical cell moving from open to closed circuit when the tip contacts the solution. In this experiment, the tip scan speed was 200 nm s^{-1} . Notice that the current flowing rapidly attains a steady-state when contact is made with the solution, consistent with the theoretical data in Figure 4.

Figure 7 demonstrates that in the force approach curve, there is a small jump to contact (tip deflection $< 5 \text{ nm}$ at $z \approx 100 \text{ nm}$) and that for smaller z , with the tip in contact with the substrate, the tip encounters a region of constant compliance. This suggests that the tip does not push significantly into the filled pore. The retract curve is linear up to the point of detachment of the tip from the solution, which is effectively instantaneous. Tip disengagement from the solution was indicated by the immediate drop to zero in both the current signal and the cantilever deflection. This phenomenon is attributed to a wetting (capillary)³³ force, F_{ad} , which acts between the tip and the solution.³⁴

The cantilever employed here was too soft to enable all the cantilever deflection–distance characteristics to be recorded on-scale. However, softer probes were preferred, because they tended to provide higher quality images of the membrane, essential for identifying isolated solution-filled pores. Cantilever deflection curves recorded with stiffer Pt-coated probes demonstrated that the retract curve was linear up to the point of detachment of the tip from solution. Thus, linear extrapolation of an off-scale cantilever force–distance curve, such as that in Figure 7a, is a valid means of estimating the adhesion force.

By measuring the magnitude of the adhesion force it is possible to estimate the effective tip contact radius at the point of pull-off. A simple schematic representation depicting this configuration is shown in Figure 8a, where R_t is the radius of curvature of the tip, ψ is the fill angle, x is the effective radius of contact between the tip and the solution, θ is the contact angle for solution on the tip, and r_1 and r_2 are the meridional and azimuthal radii of curvature of the meniscus, respectively.

(32) Schönenberger, C.; Van der Zande, B. M. I.; Fokkink, L. G. J.; Henny, M.; Schmid, C.; Krüger, M.; Bachtold, A.; Huber, R.; Birk, H.; Stauder, U. J. *Phys. Chem. B* **1997**, *101*, 5497.

(33) Israelachvili, J. N. *Intermolecular and Surface Forces*, Academic Press: San Diego, 1992, 330.

(34) (a) Thundat, T.; Zheng, X.-Y.; Chen, G. Y.; Warmack, R. J. *Surf. Sci. Lett.* **1993**, *294*, L939. (b) Weisenhorn, A. L.; Hansma, P. K.; Albrecht, T. R.; Quate, C. F. *Appl. Phys. Lett.* **1989**, *54*, 2651.

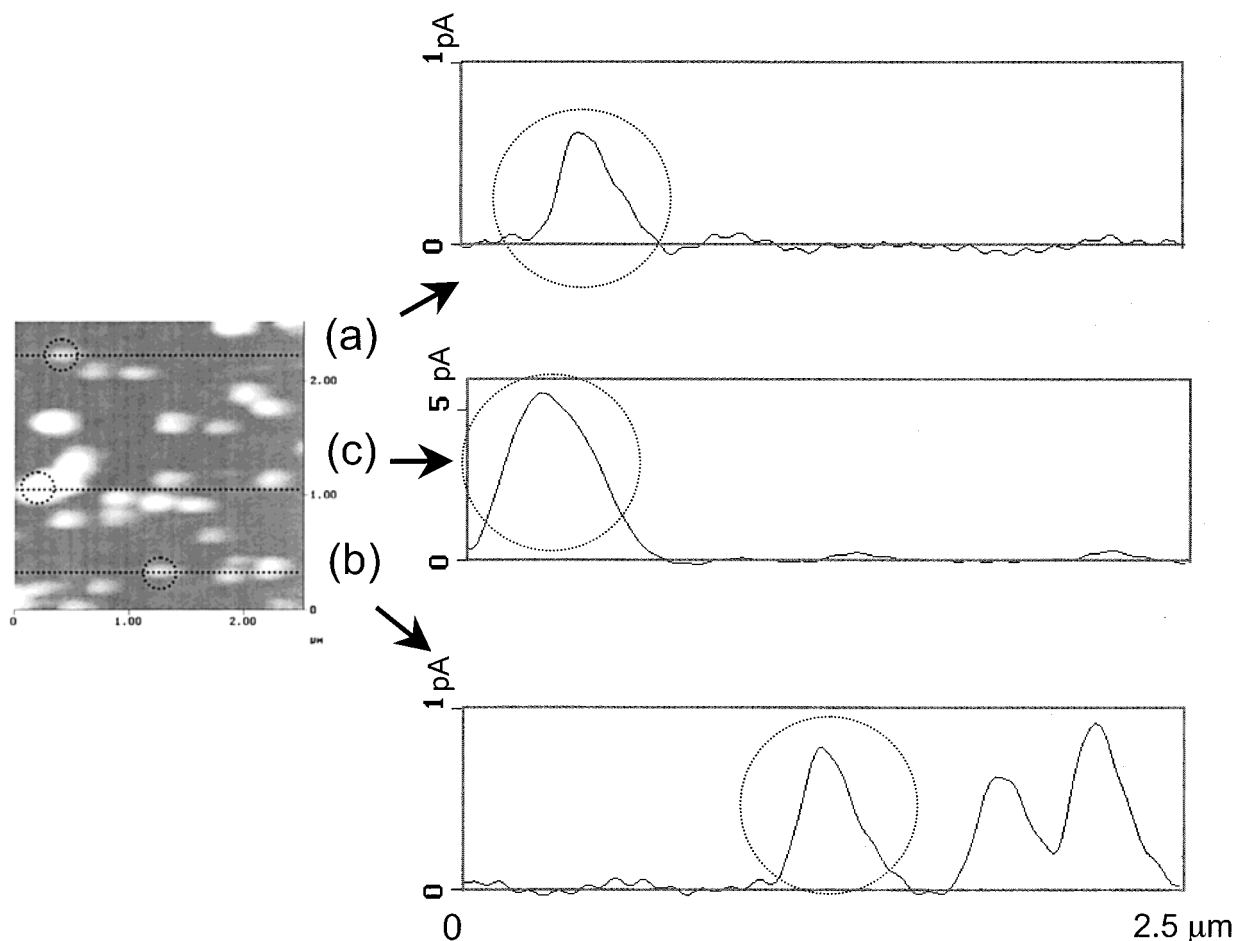


Figure 5. Cross-sectional steady-state current response across the center of (a,b) single isolated pores and (c) three pores grouped together. The solution-filled pores contained 10 mM IrCl_6^{3-} in 0.5 M KNO_3 . The tip, scanned at 1 Hz, was held at a potential of +1.0 V versus Ag/AgCl, sufficient to effect the diffusion-controlled oxidation of IrCl_6^{3-} .

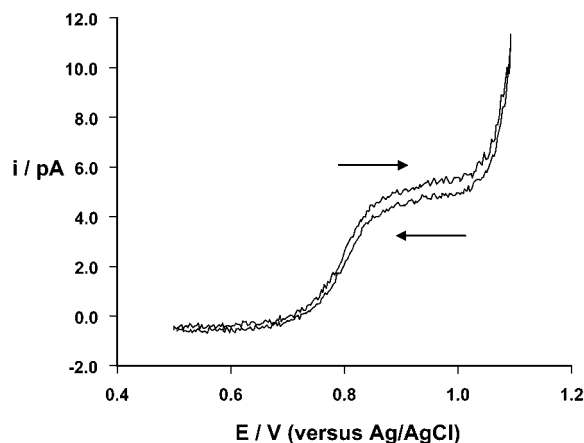


Figure 6. Cyclic voltammogram for the oxidation of 10 mM $\text{Fe}(\text{phen})_3^{2+}$ in 0.5 M KCl confined in overlapping pores at a Pt-coated AFM tip. The tip potential was scanned at a sweep rate of 10 mV s^{-1} .

The total adhesion force, F_{ad} , exerted on the tip by the solution comprises two parts:³⁵ F_t , the component of the interfacial tension force which acts tangentially to the meniscus along the contact line between the meniscus and the tip; and F_p , the force originating

from the capillary pressure difference across the curved surface of the meniscus.

$$F_{\text{ad}} = F_t + F_p \quad (4)$$

$$F_t = 2\pi R_1 \gamma_{\text{sol}} \sin(\psi) \sin(\psi + \theta) \quad (5)$$

$$F_p = -2\pi H \gamma_{\text{sol}} R_t^2 \sin^2(\psi) \quad (6)$$

In these equations, H is the local mean curvature of the tip, and γ_{sol} is the interfacial free energy of the solution. Whereas F_t can be determined exactly, the expression for H , and hence F_p , can only be solved numerically. A convenient approach known as “the circle approximation”³⁵ can be invoked in which the radial cross section of the meniscus profile is treated as the arc of a circle. The local mean curvature of the meniscus is then given by

$$H = \left(\frac{1}{r_1} + \frac{1}{r_2} \right) = \frac{1}{2R_t} \left[-\frac{\cos(\theta + \psi)}{1 - \cos(\psi)} + \frac{\sin(\theta + \psi)}{\sin(\psi)} \right] \quad (7)$$

This approximation has been used previously in the calculation of the total capillary force acting between a symmetric solid body

(35) Orr, F. M.; Scriven, L. E.; Rivas, A. P. *J. Fluid Mech.* **1975**, *67*, 732.

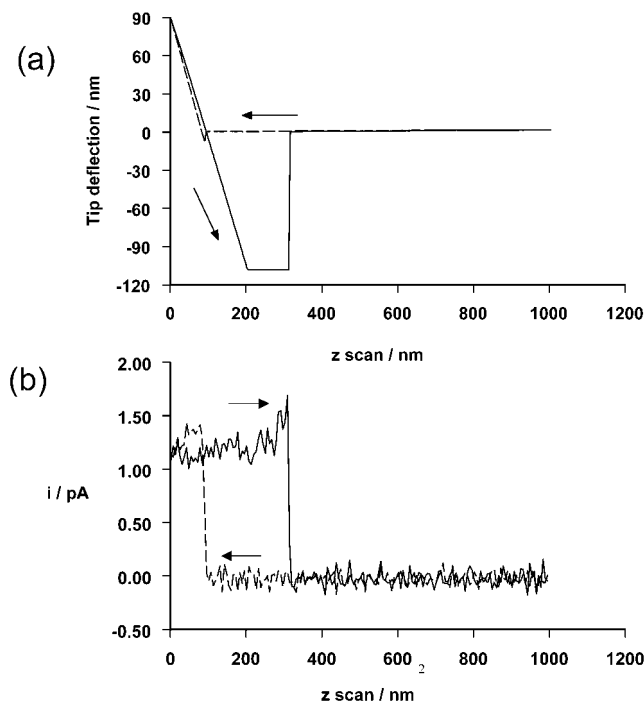


Figure 7. Cantilever deflection (a) and limiting current (b) data recorded simultaneously for the oxidation of 10 mM IrCl_6^{3-} in 0.5 M KNO_3 as an SECM-AFM tip, biased at +1.0 V versus Ag/AgCl, approached and was retracted from a solution-filled pore at a scan speed of 0.1 Hz.

and a planar surface^{36,37} and the capillary component of the pull-off force between an AFM probe and a planar substrate.³⁸

Figure 8b displays the variation of F_{ad} with x , calculated using eqs 4–7 for R_t values of 45 (lower curve), 50, and 55 nm (upper curve), which spans the range appropriate to the experiments described herein. θ , measured for aqueous electrolyte solution in contact with a polished Pt surface, was found to be 61° , in good agreement with the literature value measured under similar experimental conditions.³⁹ A value for $\gamma_{\text{sol}} = 0.072 \text{ J m}^{-2}$ was employed, which is the surface free energy of water, but this value should be close to that for an aqueous electrolyte solution. Figure 8b shows that for a given R_t value, the tip–substrate adhesion force decreases as the radius of contact increases and also that for a fixed radius of contact, the adhesion force increases with R_t . The theoretical results show that a small change in F_{ad} can lead to a large variation in x . Given the idealized geometry of the tip compared to reality (Figure 2), this approach provides only an approximate guide to the value of x .

From many force–distance retract curves recorded in separate experiments with different tips, F_{ad} was found to be in the range of 28–37 nN, suggesting electrode contact radii with a minimum value of $\sim 10 \text{ nm}$ up to a value approaching the radius of the pore. The magnitude of the measured adhesion force was found to be independent of the applied potential over the range 0.0–1.0 V versus Ag/AgCl. This observation suggests that θ is independent of applied potential, which is consistent with previous work that demonstrated that the contact angle between a drop of aqueous

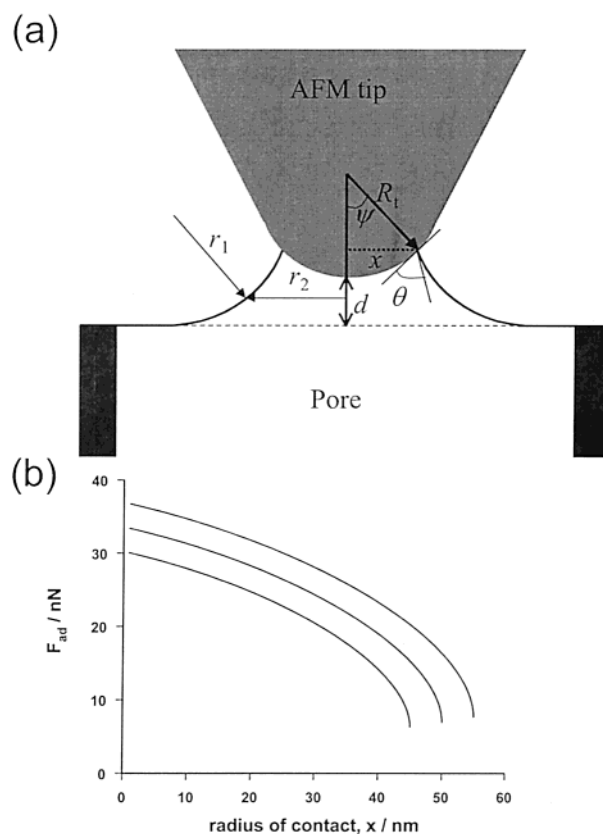


Figure 8. (a) Schematic representation of the wetting of a Pt-coated AFM tip by solution confined within a pore. R_t is the radius of curvature of the tip, ψ is the fill angle, x is the effective radius of contact between the tip and solution, θ is the contact angle for solution on the tip, and r_1 and r_2 are the meridinal and azimuthal radii of curvature of the meniscus, respectively. (b) Variation of the tip–substrate adhesion force, F_{ad} , with contact radius, x , for tips characterized by radii of curvature of 45 nm (lower curve), 50, and 55 nm (upper curve).

electrolyte and an underlying Pt electrode was independent of the applied potential investigated over the range 0.0–0.7 V versus SCE.³⁹

CONCLUSIONS

The results presented in this paper suggest a novel procedure for probing diffusional transport of electroactive target molecules through individual nanoscopic pores. The use of a Pt-coated AFM probe enables pores to be addressed electrochemically, and the underlying diffusional activity identified from a single pore. With the membrane studied, in which the thickness to pore diameter scale was 100 and the probe radius was no greater than the pore diameter, tip geometry effects were negligible. To investigate ultrathin membranes, it would be necessary to have precise knowledge of the tip geometry and contact area. Complementary force distance approach and retract curves recorded with the tip moved to and from a solution filled pore provide information on the tip current response and allow an estimation of the contact area of the tip with solution at the point of pull-off, but there is still some uncertainty in these measurements.

There is scope for using this methodology in other systems. For example, we envisage the use of in-air SECM-AFM to investigate biological materials in humid environments. This work

(36) De Lazzer, A.; Dreyer, M.; Rath, H. J. *Langmuir* **1999**, *15*, 4551.

(37) Marmur, A. *Langmuir* **1993**, *9*, 1922.

(38) Sedin, D. L.; Rowlen, K. L. *Anal. Chem.* **2000**, *72*, 2183.

(39) Willman, K. W.; Murray, R. W. *Anal. Chem.* **1983**, *55*, 1139.

would build on pure SECM studies²³ but could provide extra information on structure–activity problems with the simultaneous acquisition of force and electrochemical data.

ACKNOWLEDGMENT

J.V.M. thanks the Royal Society for the award of a University Research Fellowship. We also thank the EPSRC and Unilever Research, Port Sunlight Laboratory (Dental Division) for support. We are grateful to Mr. Phil Dobson (Department of Chemistry, University of Warwick) for help with the cantilever spring constant

calibration and contact angle experiments, and Dr. Zoë H. Barber (Department of Materials Science and Metallurgy, University of Cambridge) for platinum-coating the AFM tips used in this study. We also thank Prof. Henry White (Department of Chemistry, University of Utah) and Dr. Trevor Rayment (Department of Chemistry, Cambridge University) for helpful discussions during the course of this work.

Received for review December 20, 2001.

AC0157472